Vanadium Oxide Polycrystalline Nanorods and Ion-Exchanged Nanotubes for Enhanced Lithium Intercalation

D. McNulty[a,b,c,d], D. N. Buckley[a,b,c], and C. O'Dwyer[d,e]

[a] *Charles Parsons Initiative on Energy and Sustainable Environment, University of Limerick, Limerick, Ireland*
[b] *Department of Physics and Energy, University of Limerick, Limerick, Ireland*
[c] *Materials & Surface Science Institute, University of Limerick, Limerick, Ireland*
[d] *Department of Chemistry, University College Cork, Cork, Ireland*
[e] *Micro & Nanoelectronics Centre, Tyndall National Institute, Lee Maltings, Cork, Ireland*

In this work we investigate two alternative methods to remove amine molecules from as-synthesized vanadium oxide nanotubes (VONTs). Thermal treatment results in the formation of polycrystalline nanorods (poly-NRs) and ion exchange reactions with NaCl result in the formation of Na-VONTs. The removal of amine molecules is confirmed by monitoring the inorganic and organic phase changes and decomposition, respectively, using electron microscopy, IR spectroscopy and X-ray diffraction analyses. We compare the electrochemical performance of as-synthesized VONTs, poly-NRs and Na-VONTs. This work demonstrates that the presence of amine molecules within the layers of vanadium oxide impedes the intercalation of lithium ions, and that their removal results in a significant improvement in electrochemical characteristics. Out of the three vanadium oxide nanostructures investigated, poly- NRs exhibit the most promising results for practical use as a cathode material.

Introduction

In recent years there has been an incredible upsurge in the research of developing next generation lithium ion batteries with higher capacities and increased energy densities. (1-9) Recently lithium-ion batteries have penetrated the market of hybrid and electrical vehicles. (10-12) Over the last decade the technological advancements which have led to these products have been outstanding and currently battery technology is just about keeping up. In order to meet the power and energy demands of future devices, every aspect of lithium ion batteries must be developed and enhanced. There is currently a tremendous amount of research being made into possible cathode materials to replace the most commonly currently used materials. (13-16) Vanadium oxide was first proposed as cathode material as far back as the 1970's (17), however, the micron sized particles available at the time offered limited electrochemical performance. (18)

Vanadium oxide nanotubes (VONTs) were first reported in 1998 by Spahr et al. (19) and since then has been a great deal of research into how to fully optimize them as a cathode material for lithium ion batteries. (20-24) Typically VONTs are prepared by hydrothermal treatment of a vanadium oxide precursor mixed with a primary amine. (25, 26) The amine molecules are crucial

to the formation of the VONTs as they maintain the vanadium oxide layers which scroll to form the nanotube structure. (27, 28) While the amines are vital in the synthesis of the VONTs they are unfortunately detrimental in their electrochemical performance. (29) It has been proposed that the amine molecules occupy the majority of the possible lithium intercalation sites within the VONTs and hence are responsible for the poor cycling performance which has been reported for as-synthesized VONTs. (30, 31)

In this work we investigate two alternative methods to remove the amine molecules from the as-synthesized VONTs, using the nanotube structure as a 'backbone' or 'starting structure' for other polymorphs, while retaining nanoscale crystalline structure. The first method consists of annealing as-synthesized VONTs to high temperatures (~ 600 ^{o}C) in an effort to evaporate the amines out of the vanadium oxide structure. Thermal treatment of VONTs results in a specific structural transformation to vanadium oxide polycrystalline nanorods (poly-NRs) during annealing. The second method is an ion exchange process. As-synthesized VONTs undergo an ion exchange treatment to partially substitute ionized amine head groups with Na^{+} ions.

We confirm the removal of amine molecules by monitoring the inorganic and organic phase changes and decomposition, respectively, using IR spectroscopy, electron microscopy and X-ray diffraction analyses. Through detailed electrochemical investigations without influence from polymeric binders nor conductive additives, we compare the electrochemical performance of as-synthesized VONTs, poly-NRs and Na-VONTs. This work demonstrates that the heavy functionalization of VONTs by amine molecules impedes the intercalation of lithium ions, and that their removal results in a significant improvement in electrochemical characteristics. The electrochemical performance of ion exchanged VONTs was greatly enhanced by the removal of amine molecules, while still maintaining the nanotube structure. However, the poly-NRs exhibit the most promising results for practical use as a cathode material.

Experimental

Vanadium oxide nanotubes were synthesized by hydrothermal treatment of a mixture of vanadium oxide xerogel and a primary amine, following usual procedures. (27, 32, 33) A nonylamine organic template was used in a molar ratio of xerogel to amine of 1:2, with 3 ml of ethanol added per gram of xerogel. This molar ratio of xerogel to amine was chosen as it was found to be the optimum ratio resulting in the highest yield of high quality VONTs. (34) The poly-NRs for electrochemical testing were prepared by thermally treating VONT powder in a quartz glass furnace which was heated from room temperature to 600 ^{o}C at 5 ^{o}C min^{-1} in a nitrogen atmosphere. Na-VONTs were prepared using previously reported methods. (35, 36) NaCl was added to as-synthesized VONTs in a molar ratio of (4:1). This was then stirred in a mixture of ethanol and distilled water which were mixed in a molar ratio of 4:1 with 0.2 ml/mg of VONTs.

TEM analysis including bright field and electron diffraction was conducted using a JEOL JEM-2100F TEM operating at 200 kV. SEM analysis was performed using a Hitachi S-4800 at an accelerating voltage of 10 kV. Thermogravimetric analysis (TGA) was carried out using a Perkin Elmer TGA. Samples for TGA were placed in an alumina crucible and heated to 600 ^{o}C at a heating rate of 5^{o}C min^{-1} and then cooled, in a nitrogen atmosphere. Fourier transform infrared spectroscopy (FTIR) was conducted on Perkin Elmer series 2000 apparatus in the region of 4000-650 cm^{-1}. X-Ray Diffraction (XRD) was performed using an X'pert MRDpro Panalytical

diffractometer with Cu Kα radiation (Cu Kα, λ = 0.15418 nm, operation voltage 40 kV, current 30 mA).

The electrochemical properties of VONTs, poly-NRs and Na-VONTs were investigated using a three electrode cell. The cells were assembled in inside a glovebox under an argon atmosphere. The electrolyte consisted of a 1 mol dm^{-3} solution of $LiPF_6$ salt in a 1:1 (v/v) mixture of ethylene carbonate (EC) in dimethyl carbonate (DMC). The working electrodes were prepared by dropping a sonicated mixture of the active material powder and ethanol on to a stainless steel foil substrate which was subsequently dried in a vacuum oven at 100 ^oC for 2 hours. No additional conductive additives or binders were added to the various vanadium oxide working electrodes, allowing direct electrochemical examination of the various structures without complications from conductive additives and non-uniform mixtures. The counter and reference electrodes were pure lithium metal. Both working and counter electrodes had a geometric surface area of 1 cm^2. Galvanostatic discharge/charge tests were performed using a CH Instruments model 605B potentiostat/galvanostat in a potential window of 4.0 V – 1.2 V with a constant current of ± 30 μA. Energy density values were calculated based on the average potential from the upper and lower potential limits.

Results and Discussion

The thermal stability of VONTs was studied by thermogravimetric analysis under a nitrogen atmosphere. The resulting mass loss curve is shown in Figure 1. Less than 1% mass is lost when VONTs are heated to 100 ^oC. Significant mass losses begin to occur when the VONTs are heated above ~ 120 ^oC as indicated by the knee in curve, associated with the removal of physisorbed and chemisorbed water present within the VONTs. There is one major loss of ~ 52% mass which occurs between 120 and 450 ^oC due to decomposition of amine molecules which were present within the layers of vanadium oxide

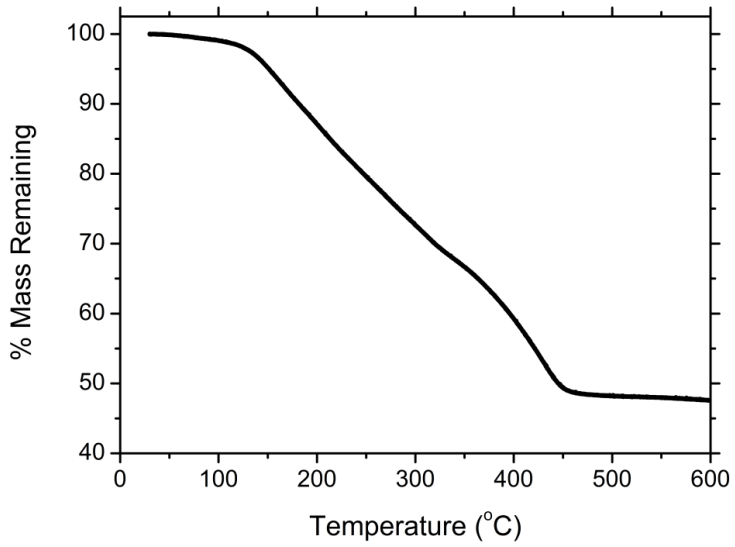

Figure 1 TGA curves for as-synthesized VONTs and Na-VONTs heated to 600 ^oC at a heating rate of 5 K/min.

VONTs are typically prepared by the hydrothermal treatment of a vanadium oxide precursor mixed with primary amines. During the synthesis procedure for VONTs organic amines are intercalated between the layers of vanadium oxide. In the initial aging stage the amines are hydrolyzed by water to form ammonium ions and hydroxide ions (37). The resulting hydroxide ions break down the V=O bond present in the V_2O_5 molecule to form (V–OH) and ($V–O^-$) bonds. The attachment of the amine is generally accepted to be an electrostatic bond between the ionized amino head group (NH_3^+) and the ($V–O^-$) bond (32, 38). During the ion exchange reaction the positively charged amine head group is exchanged with a Na^+ ion (35). This exchange is likely to be a partial substitution (39, 40) as illustrated in Figure 2. The bilayer of primary amines form a structure maintaining template hence, without a partial presence of amines, Na-VONTs would most likely not retain their tubular morphology.

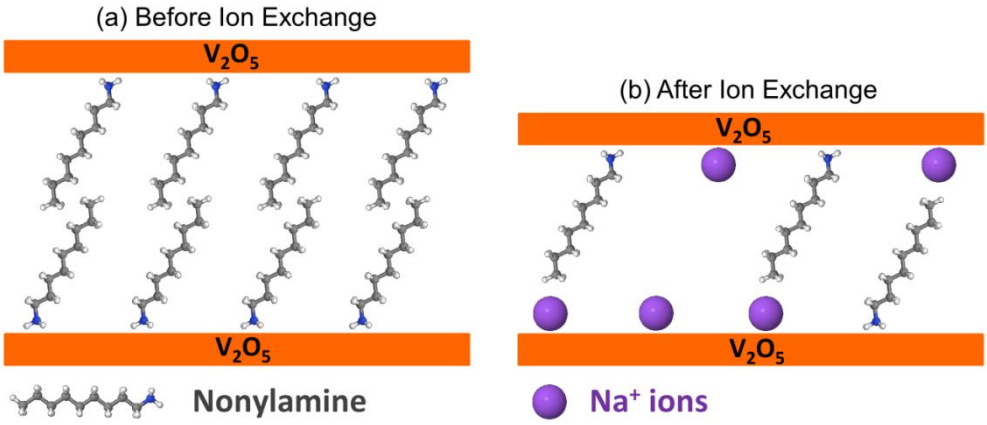

Figure 2 Simplified schematic demonstrating the partial substitution of ionized nonylamine head groups with Na^+ ions (a) before and (b) after ion exchange

TEM images of VONTs, poly-NRs and Na-VONTs are shown in Figure 3 (a) – (c), respectively. There are three main features present in the structure of as-synthesized VONTs, (25) as can be seen in Figure 3 (a). These are (i) the hollow core running through the nanotube, (ii) the layered walls on either side of the hollow core and (iii) the tube openings at both ends. When as-synthesized VONTs are annealed to high temperatures, the organic amines which are present within the layers of vanadium oxide are removed and a structural rearrangement occurs. The pristine nanotubes collapse to form poly-crystalline nanorods. (41) Poly-NRs are an agglomeration of nanocrystallites of vanadium oxide, as shown in Figure 3 (b). After ion exchange the as-synthesized VONTs maintain their nanotubular structure, as seen in Figure 3 (c). Na-VONTs also retain the characteristic nanotubular features. However, in comparison with as-synthesized VONTs the interlayer spacings seen in the layered walls of the Na-VONTs are narrower. The interlayer spacing for as-synthesized VONTs was estimated to be ~2.74 nm from a range of HRTEM images. After Na-ion exchange, the interlayer spacing dimension decreased to ~1.09 nm. This is due to the substitution of nonylamine molecules with much smaller Na^+ ions. Previous density functional theory analysis of the amine bilayer molecular packing and the stability of the interlayer spacing in vanadium oxide nanotube confirm that bending conformations are possible for amine that can entropically fill adjoining free space on each

juxtaposed face of the vanadium oxide layer. Ion-exchange removal of amines can cause pockets of free space that allows alkyl chain bending, which would contribute to a net narrowing of the interlayer spacing. Also, the inner diameter of the Na-VONTs is wider than the as-synthesized VONTs. This is due to a combination of effects which occur as a result of the ion exchange reaction. SEM images of VONTs, poly-NRs and Na-VONTs are shown in Figure 3 (a) – (c), respectively. The as-synthesized VONTs have smooth outer walls and distinct tube openings as can be seen in Figure 3 (a). Similarly the tube openings for Na-VONTs are quite visible. The tube walls have much rougher edges (Figure 3 (c)). The nanotubes maintain their tubular structure after ion exchange reactions.

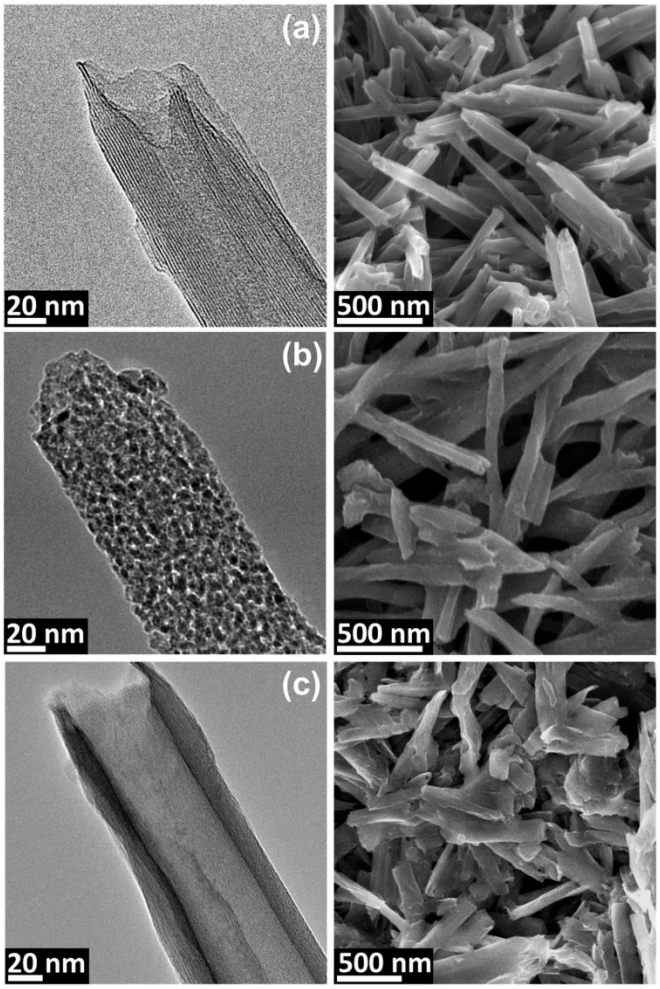

Figure 3 TEM (left) and SEM images (right) of (a) as-synthesized VONTs, (b) poly-NRs and (c) Na-VONTs.

FTIR measurements were carried out to verify to partial exchange of amine molecules with Na^+ ions and to determine the effects of thermal treatment on as-synthesized VONTs. The FTIR spectra for orthorhombic bulk V_2O_5, as-synthesized VONTs, poly-NRs and Na-VONTs are shown in Figure 4. The characteristic vanadyl band (V=O) for crystalline V_2O_5 can be seen at 982 cm^{-1} as can be seen in Figure 4. (42, 43) For as-synthesized VONTs, poly-NRs and Na-

VONTs there is a small shift of the vanadyl band to higher frequencies (~ 992 cm^{-1}). This is due to electrostatic interactions between the intercalates and the host structure known to be characteristic of an increased V^{4+} quantity. (40, 44) As can be seen in Figure 4, a significant difference in the V=O, V-O and V-O-V vibrations of the various samples is observed after ion exchange.

The nonylamine molecules present within the vanadium oxide layers of the as-synthesized VONTs are also responsible for peaks observed in the FTIR spectra. The peaks observed at 2850 and 2920 cm^{-1} are due to symmetric and asymmetric stretching vibrations for CH_2 groups of the primary alkyl chain. (42, 45-47) The other peaks observed in this region are due to symmetric and asymmetric stretching vibrations for terminal CH_3 groups, observed at 2870 and 2955 cm^{-1} respectively. The absorbance cross-section is greater for the alkyl chain containing 8 CH_2 groups (nonylamine), and compared to the terminal CH_3 group, has a higher IR absorbance intensity in a well-defined amine bilayer, and the spectra can be seen in Figure 4. The wide band observed from 3050 – 3250 cm^{-1} is due to N-H vibrations present from the NH_2 head group of the amine chain. (48) These peaks were not observed for the bulk and poly-NR sample, as expected. Heating as-synthesized VONTs to 600 ^oC removes the amine molecules from the VONTs and results in a structural rearrangement as verified through TGA and TEM imaging. A limited absorbance from symmetric and asymmetric C-H stretching and bending modes and N-H vibrations were observed for Na-VONTs. This would suggest that there has been an effective removal of amine molecules after the ion exchange reactions. As the Na-VONTs retain their nanotube structure, it is likely that, after ion exchange a small quantity of amine molecules remain within the layers of vanadium oxide. A low intensity peak is observed in the FTIR spectrum for Na-VONTs ~2920 cm^{-1}, indicating that some amine molecules remain after ion exchange. This can be seen in the magnified region of the Na-VONTs spectrum in Figure 4 (i).

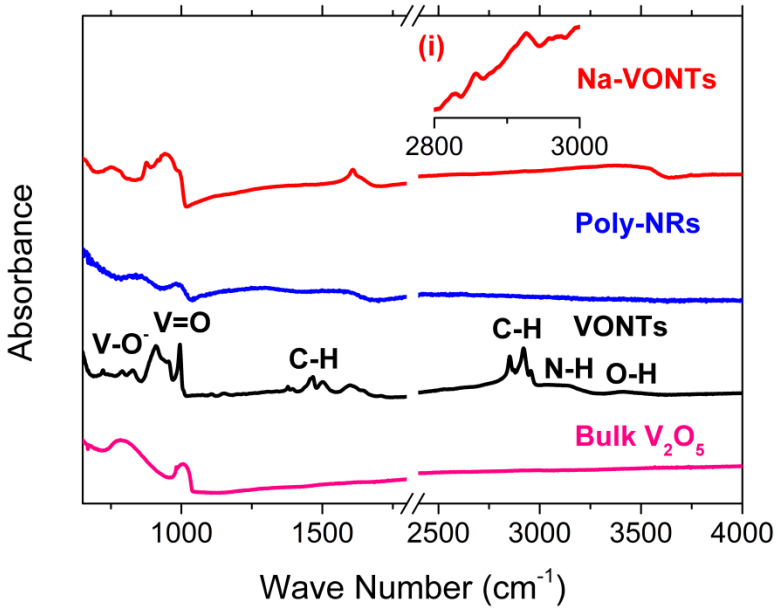

Figure 4 FTIR spectra for bulk V_2O_5 powder, as synthesized VONTs, poly-NRs and Na-VONTs. (i) Magnified region of Na-VONTs spectrum from 2700 – 3400 cm^{-1}.

The XRD patterns of bulk V_2O_5, as synthesized VONTs, poly-NRs and Na-VONTs are shown in Figure 5. The low angle region in Figure 5 (a) shows (00*l*) Bragg reflection peaks for each vanadium oxide sample. The d-spacing of {001} peak corresponds to the spacing between the layers of vanadium oxide within the crystal lattice. The measured interlayer distance for orthorhombic V_2O_5 was ~0.98 nm. After hydrothermal treatment, amines are intercalated between the vanadium oxide layers and VONTs are formed, the d-spacing (for the crystallographic c-axis) for as-synthesized VONTs increases to ~2.73 nm, due to widening caused by a bilayer of interdigitated amines on juxtaposed V_2O_5 faces. After ion exchange, the majority of the nonylamine molecules have been replaced with Na^+ ions. The length of a single nonylamine molecule is ~1.33 nm and the ionic radius of Na^+ is ~0.116 nm. Hence there is a decrease in the interlayer spacing for the ion exchange product. The resulting interlayer spacing for Na-VONTs is ~1.09 nm. The variation in interlayer spacing for each sample is demonstrated by the shift in the {001} peak for bulk V_2O_5 to a lower angle for as-synthesized VONTs; a shift to higher angles is found for Na-VONTs, as shown in Figure 5(a).

The second region shown in Fig. 6.10(b) comprises (*hk*0) reflections, characteristic of the crystal structure of V_2O_5 (27, 28, 32, 33, 49). A characteristic of curved single crystals is a 'Fano-type' lineshape (27); in VONTs, this is indicative of the high structural order of a scrolled VONT. A series of 'Fano-type' peaks were observed in the diffraction pattern for as-synthesized VONTs, including (210), (310), (320) and (420) peaks. These peaks are broadened for poly-NRs due to a reduction in crystalline order within the scrolls making up the VONT. This has been verified through TEM imaging the VONTs as shown in Figure 3, and is consistent with a removal of the structure-maintaining organic template as determined by FTIR measurements in Figure 4. After ion exchange the Na-VONTs contain Na^+ ions between layers of vanadium oxide via intercalation from solution. This results in a modification of the crystal structure from an orthorhombic system to a monoclinic system, with cell parameters closely matching those of NaV_6O_{15}. (50)

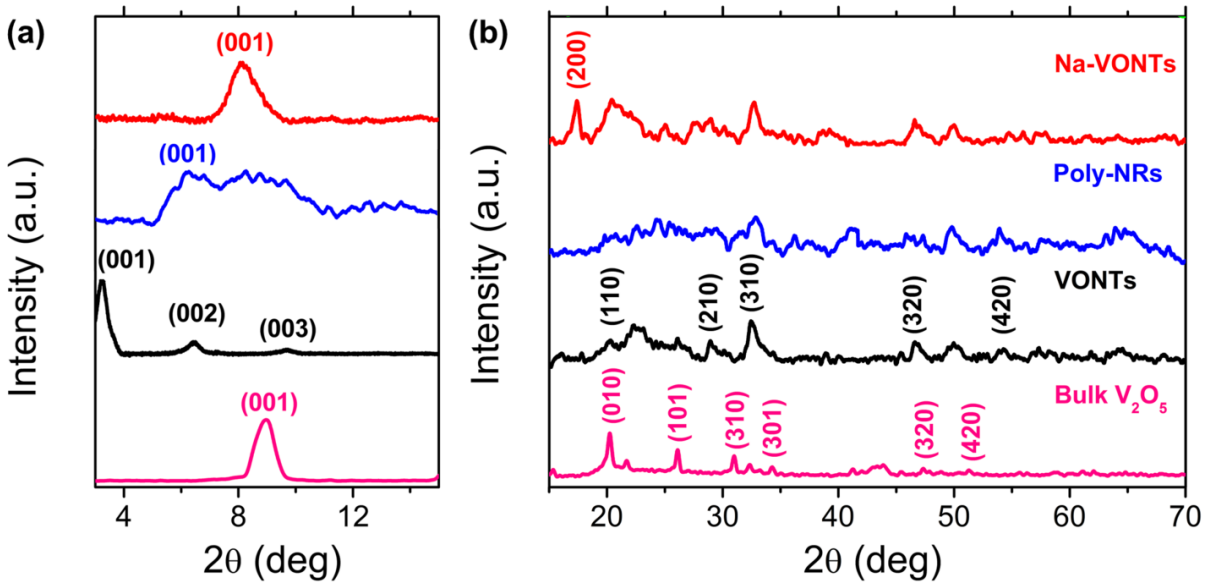

Figure 5 Comparison of XRD patterns obtained for bulk V_2O_5, as synthesized VONTs, poly-NRs and Na-VONTs: (a) (00*l*) reflections (b) (*hk*0) reflections.

The discharge/charge curves for each vanadium oxide nanostructures after the second cycle are shown in Figure 6. For as-synthesized VONTs ~0.04 mol of lithium was intercalated after the 2nd discharge, however only ~0.01 mol of lithium was successfully removed, as shown in Figure 6 (a). This indicates that the insertion and removal of Li^+ ions is not highly reversible for as-synthesized VONTs. The single phase transition which can be seen in the discharge curves for as-synthesized VONTs is due to the formation of the α-phase ($\chi \geq 0.01$). Poly-NRs demonstrate a high level of reversibility, as can be seen in Figure 6 (b). After the 2nd discharge ~1.3 mol of lithium was intercalated into the poly-NR sample, during the 2nd charge ~1.2 mol of lithium was successfully removed. Interestingly out of the three vanadium oxide samples investigated, the highest content of reversibly intercalated lithium is possible with the poly-NRs. The cycling performance for Na-VONTs shown in Figure 6 (c) highlights the benefits of removing amine molecules to improving electrochemical performance. After ion exchange more lithium ions can be inserted and removed. After the 2nd discharge ~0.7 mol of lithium was inserted and ~0.35 mol was successfully removed after the 2nd charge.

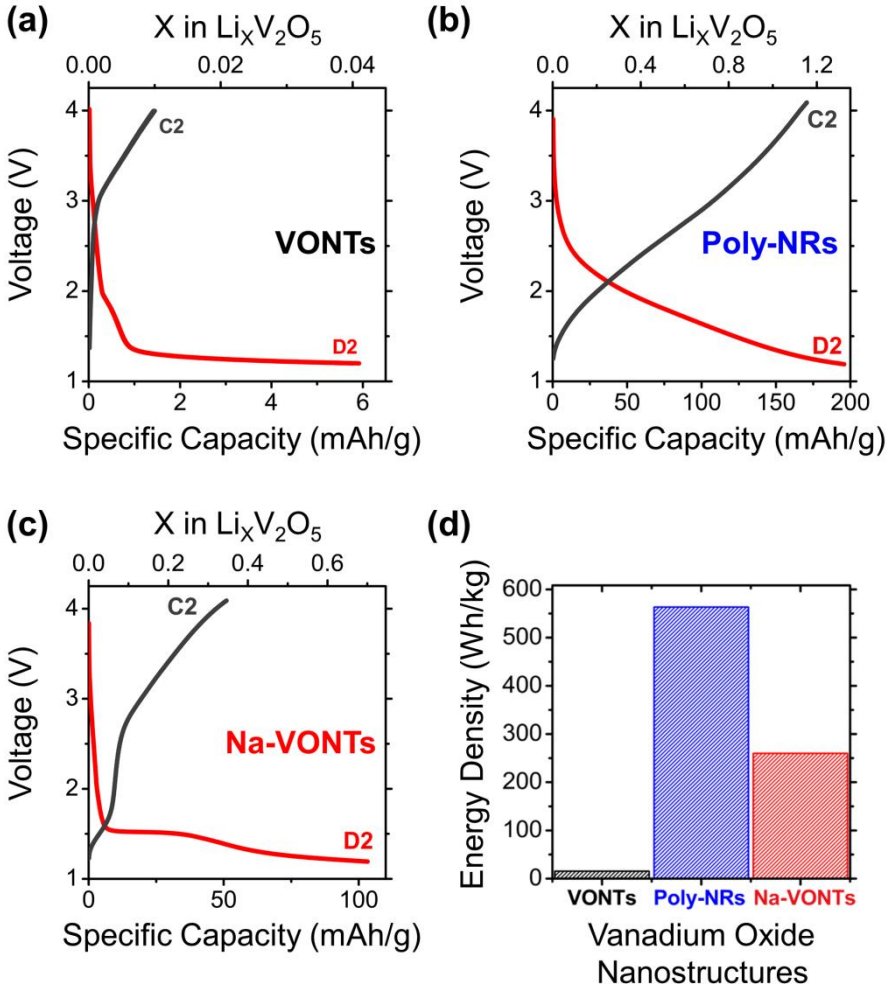

Figure 6 2nd discharge/charge curves for (a) VONTs (b) Poly-NRs and (c) Na-VONTs; (d) Energy density values calculated after the second discharge for VONTs, Poly-NRs and Na-VONTs.

The profile of the discharge/charge curves offer an insight into the lithium insertion mechanism which occurs for each sample. The discharge curves for as-synthesized VONTs and Na-VONTs have plateaus at ~1.4 and ~1.5 V respectively, indicating that the majority of the lithium insertion begins to occur at these potentials. The discharge/ charge curves for poly-NRs sample do not show any discrete phase transitions, instead they are smooth curves, as shown in Figure 6 (b). This is typically indicative of an amorphous material. The overall poly-NR structure responds electrochemically as an amorphous-like phase undergoing lithiation. However TEM imaging and XRD analysis verify that poly-NRs are indeed polycrystalline on the nanoscale (2-10 nm crystallites). Similar smooth cycling curves were reported for vanadium oxide xerogels which were heated to 300 ^{o}C (51).

Energy densities for VONTs, poly-NRs and Na-VONTs are shown in Figure 6 (d). It is immediately clear that poly-NRs achieved by far the highest energy density with a value of ~565 Wh/kg. Na-VONTs achieved an energy density of ~260 Wh/kg, whereas the as-synthesized VONTs achieved an energy density of ~15 Wh/kg. These calculated energy density values are further evidence of the superior electrochemical performance of poly-NRs over the other vanadium oxide nanostructures investigated.

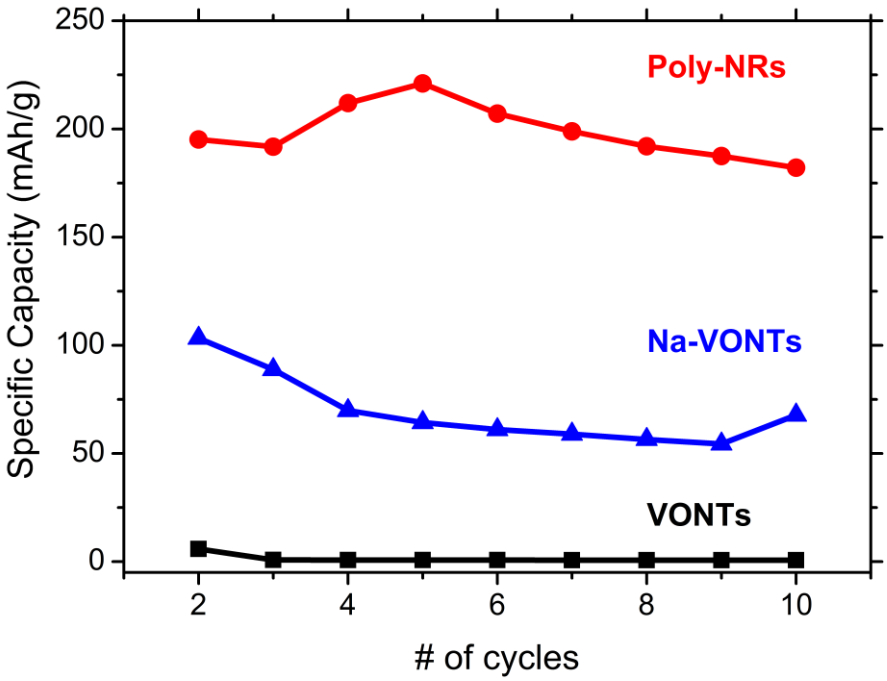

Figure 7 Specific capacities for VONTs, poly-NRs and Na-VONTs obtained during 10 cycles.

The specific capacity values obtained for each vanadium oxide nanostructure over the first 10 cycles are shown in Figure 7. The capacity for as-synthesized VONTs immediately drops to < 1 mAh/g, indicating that the intercalation of lithium ions for this sample is not a reversible reaction. After the 2nd discharge the capacity was 195 mAh/g for the poly-NRs. This marginally decreased to 182 mAh/g after the 10th discharge, corresponding to a ~93 % retention in the initial capacity. The superior performance of the poly-NRs is due to the removal of amine molecules and the structural conversion from VONTs to poly-NRs comprised of nanocrystals of V_2O_5. For

Na-VONTs, after the 2nd discharge the capacity was ~103 mAh/g, this decreased to 68 mAh/g after the 10th discharge, corresponding to a ~63% retention in the initial capacity. This is a substantial loss in capacity but also a significant improvement over the as-synthesized VONTs. The improved electrochemical performance of Na-VONTs over as-synthesized VONTs is due to the partial substitution of amine molecules with Na^+ ions.

Conclusions

It was proposed that amine molecules intercalated between the layers of vanadium oxide may occupy possible lithium intercalation sites. Strategies to remove amine molecule templates from as-synthesized VONTs included thermal treatment (thermolytic decomposition of amines) and Na-ion exchange reactions. Through thermogravimetric analysis (TGA) it was found that the organic amine template can be efficiently removed from the VONTs by heating to 600 ºC. When as-synthesized VONTs are annealed to 600 ºC in an inert atmosphere a structural transition from pristine nanotube to polycrystalline nanorod occurs.

As-synthesized VONTs were the subject of ion-exchange reactions with a solution of NaCl in ethanol and water, to remove amine molecules. During solution treatment, NH_3^+ amine head groups were substituted with Na^+ ions. The exchange was a partial substitution as the resulting Na-VONTs maintained the initial tubular structure of the as-synthesized material. FTIR analysis confirmed the reduced amount of amine molecules present after ion exchange.

The electrochemical performance of each vanadium oxide nanostructure was compared through galvanostatic cycling. VONTs containing amines suffer from severe capacity fading and miniscule specific capacities. After ion exchange, the specific capacities for Na-VONTs increased dramatically compared to the as-synthesized material, due to the removal of amines. The greatest improvement in electrochemical performance compared to as-synthesized VONTs was achieved with poly-NRs. Poly-NRs no longer contain the undesirable amine molecules but also maintain a similar aspect ratio to the as-synthesized VONTs in a polycrystalline structure comprising V_2O_5 nanocrystals. Hence poly-NRs benefit from all of the advantages associated with nanostructured electrode materials. Poly-NRs also demonstrated significant capacity retention over 10 cycles, with an associated energy density of ~565 Wh/kg. The enhanced performance of poly-NRs over other vanadium oxide nanostructures which were tested is most likely due to the combination of the removal of amine molecules and the structural rearrangement from pristine nanotubes to polycrystalline nanorods.

Acknowledgements

This publication has emanated from research conducted with the financial support of the Charles Parsons Initiative and Science Foundation Ireland (SFI) under Grant No. 06/CP/E007. Part of this work was conducted under the framework of the INSPIRE programme, funded by the Irish Government's Programme for Research in Third Level Institutions, Cycle 4, National Development Plan 2007-2013. We also thank the Materials and Surface Science Institute (MSSI) at the University of Limerick for access to TEM, TGA and FTIR. We acknowledge support from a SFI Stokes Award under contract no. 07/SK/B1232a and a Technology Innovation and Development Award under contract no 13/TIDA/E2761.

References

1. J. M. Tarascon and M. Armand, *Nature*, **414**, 359 (2001).
2. P. Poizot, S. Laruelle, S. Grugeon, L. Dupont and J. Tarascon, *Nature*, **407**, 496 (2000).
3. A. S. Arico, P. Bruce, B. Scrosati, J.-M. Tarascon and W. van Schalkwijk, *Nat. Mater.*, **4**, 366 (2005).
4. P. G. Bruce, B. Scrosati and J.-M. Tarascon, *Angew. Chem. Int. Edit.*, **47**, 2930 (2008).
5. M. Osiak, H. Geaney, E. Armstrong and C. O'Dwyer, *J. Mater. Chem. A*, **2**, 9433 (2014).
6. M. S. Islam and C. A. Fisher, *Chem. Soc. Rev.*, **43**, 185 (2014).
7. M. Hu, X. Pang and Z. Zhou, *J. Power Sources*, **237**, 229 (2013).
8. Y.-Y. Hu, Z. Liu, K.-W. Nam, O. J. Borkiewicz, J. Cheng, X. Hua, M. T. Dunstan, X. Yu, K. M. Wiaderek and L.-S. Du, *Nat. Mater.*, **12**, 1130 (2013).
9. Z. Chen, Y. Ren, A. N. Jansen, C.-K. Lin, W. Weng and K. Amine, *Nat. Commun.*, **4**, 1513 (2013).
10. L. Lu, X. Han, J. Li, J. Hua and M. Ouyang, *J. Power Sources*, **226**, 272 (2013).
11. C. Arbizzani, L. Damen, M. Lazzari, F. Soavi and M. Mastragostino, *Lithium Batteries: Advanced Technologies and Applications*, **265** (2013).
12. E. Karden, S. Ploumen, B. Fricke, T. Miller and K. Snyder, *J. Power Sources*, **168**, 2 (2007).
13. D. Liu, W. Zhu, J. Trottier, C. Gagnon, F. Barray, A. Guerfi, A. Mauger, H. Groult, C. Julien and J. Goodenough, *RSC Advances*, **4**, 154 (2014).
14. G. Kucinskis, G. Bajars and J. Kleperis, *J. Power Sources*, **240**, 66 (2013).
15. B. Xu, D. Qian, Z. Wang and Y. S. Meng, *Materials Science and Engineering: R: Reports*, **73**, 51 (2012).
16. J. W. Fergus, *J. Power Sources*, **195**, 939 (2010).
17. M. S. Whittingham, *J. Electrochem. Soc.*, **123**, 315 (1976).
18. J. M. Cocciantelli, M. Ménétrier, C. Delmas, J. P. Doumerc, M. Pouchard, M. Broussely and J. Labat, *Solid State Ionics*, **78**, 143 (1995).
19. M. E. Spahr, P. Bitterli, R. Nesper, M. Müller, F. Krumeich and H. U. Nissen, *Angew. Chem. Int. Edit.*, **37**, 1263 (1998).
20. S. Nordlinder, K. Edström and T. Gustafsson, *Electrochem. Solid-State Lett.*, **4**, A129 (2001).
21. S. Nordlinder, L. Nyholm, T. Gustafsson and K. Edström, *Chem. Mater.*, **18**, 495 (2005).
22. M. L.-Q. Chen Wen, Xu Qing, J.-F. Peng, Q.-Y. Zhu, *Chemical Journal of Chinese Universities*, **25**, 904 (2004).
23. C.-J. Cui, G.-M. Wu, J. Shen, B. Zhou, Z.-H. Zhang, H.-Y. Yang and S.-F. She, *Electrochim. Acta*, **55**, 2536 (2010).
24. H. X. Li, L. F. Jiao, H. T. Yuan, M. Zhang, J. Guo, L. Q. Wang, M. Zhao and Y. M. Wang, *Electrochem. Commun.*, **8**, 1693 (2006).
25. M. E. Spahr, P. Stoschitzki-Bitterli, R. Nesper, O. Haas and P. Novák, *J. Electrochem. Soc.*, **146**, 2780 (1999).
26. H. J. Muhr, F. Krumeich, U. P. Schönholzer, F. Bieri, M. Niederberger, L. J. Gauckler and R. Nesper, *Adv. Mater.*, **12**, 231 (2000).
27. F. Krumeich, H. J. Muhr, M. Niederberger, F. Bieri, B. Schnyder and R. Nesper, *J. Am. Chem. Soc.*, **121**, 8324 (1999).
28. C. O'Dwyer, D. Navas, V. Lavayen, E. Benavente, M. A. S. Ana, G. González, S. B. Newcomb and C. M. S. Torres, *Chem. Mater.*, **18**, 3016 (2006).

29. D. McNulty, D. Buckley and C. O'Dwyer, *J. Electrochem. Soc.*, **161**, A1321 (2014).
30. A. I. Popa, E. Vavilova, C. Täschner, V. Kataev, B. Büchner and R. d. Klingeler, *J. Phys. Chem. C*, **115**, 5265 (2011).
31. D. McNulty, D. N. Buckley and C. O'Dwyer, *J. Power Sources*, **267**, 831 (2014).
32. X. Chen, X. Sun and Y. Li, *Inorg Chemistry*, **41**, 4524 (2002).
33. G. T. Chandrappa, N. Steunou, S. Cassaignon, C. Bauvais and J. Livage, *Catal. Today.*, **78**, 85 (2003).
34. D. McNulty, D. N. Buckley and C. O'Dwyer, *ECS Trans.*, **35**, 237 (2011).
35. J. M. Reinoso, H. J. Muhr, F. Krumeich, F. Bieri and R. Nesper, *Helvetica Chimica Acta*, **83**, 1724 (2000).
36. S. Nordlinder, J. Lindgren, T. Gustafsson and K. Edström, *J. Electrochem. Soc.*, **150**, E280 (2003).
37. C. O'Dwyer, V. Lavayen, D. A. Tanner, S. B. Newcomb, E. Benavente, G. Gonzalez and C. M. S. Torres, *Adv. Func. Mater.*, **19**, 1736 (2009).
38. P. Liu, I. L. Moudrakovski, J. Liu and A. Sayari, *Chem. Mater.*, **9**, 2513 (1997).
39. J. Cao, J. Musfeldt, S. Mazumdar, N. Chernova and M. Whittingham, *Nano. Lett.*, **7**, 2351 (2007).
40. M. Malta, G. Louarn, N. Errien and R. M. Torresi, *J. Power Sources*, **156**, 533 (2006).
41. D. McNulty, D. N. Buckley and C. O'Dwyer, *ECS Trans.*, **50**, 165 (2013).
42. W. Chen, J. Peng, L. Mai, Q. Zhu and Q. Xu, *Mater. Lett.*, **58**, 2275 (2004).
43. B. Azambre, M. Hudson and O. Heintz, *J. Mater. Chem.*, **13**, 385 (2003).
44. M. Armand and J. M. Tarascon, *Nature*, **451**, 652 (2008).
45. J. Liu, X. Wang, Q. Peng and Y. Li, *Adv. Mater.*, **17**, 764 (2005).
46. C. O'Dwyer, G. Gannon, D. McNulty, D. N. Buckley and D. Thompson, *Chem. Mater.*, **24**, 3981 (2012).
47. F. Sediri, F. Touati and N. Gharbi, *Mater. Lett.*, **61**, 1946 (2007).
48. A. Dobley, K. Ngala, S. Yang, P. Y. Zavalij and M. S. Whittingham, *Chem. Mater.*, **13**, 4382 (2001).
49. A. V. Grigorieva, E. A. Goodilin, A. V. Anikina, I. V. Kolesnik and Y. D. Tretyakov, *Mendeleev Communications*, **18**, 71 (2008).
50. H. Liu, Y. Wang, L. Li, K. Wang, E. Hosono and H. Zhou, *J. Mater. Chem.*, **19**, 7885 (2009).
51. K. West, B. Zachau-Christiansen, T. Jacobsen and S. Skaarup, *Electrochim. Acta*, **38**, 1215 (1993).